Lattice Boltzmann modeling of liquid clusters in granular media

Jean-Yves Delenne
IATE, UMR 1208 INRA-CIRAD-Montpellier Supagro-University Montpellier 2
Montpellier, France

Vincent Richefeu
3SR, UMR 5521 UJF-Grenoble 1, Grenoble-INP, CNRS UMR 5521
Grenoble, France

Farhang Radjai
LMGC, UMR 5508 CNRS-University Montpellier 2
Montpellier, France

ABSTRACT: We use capillary condensation simulated by a multiphase Lattice Boltzmann model as a means to generate homogeneous distributions of liquid clusters in 2D granular media. Liquid droplets condense from the vapor phase between and on the grains, and they transform into capillary bonds and liquid clusters as thermodynamic equilibrium is approached. As the amount of condensed liquid is increased, liquid clusters of increasing connectivity are formed and the distribution of liquid undergoes topological transitions until the whole pore space is filled by the liquid. We investigate the cluster statistics and local grain environments. From extensive simulations, we also obtain the mean Laplace pressure as a function of the amount of liquid, which is found to be quite similar to the well-known experimental retention curve in soil mechanics.

1 INTRODUCTION

In soil mechanics and powder technology, granular materials are often filled by a wetting or binding liquid that plays a key role in their rheological properties. For example, the triggering of landslides and sediment transport involve the rheology of dense mixtures of grains and water (Iverson, Reid, Iverson, LaHusen, Logan, Mann, & Brien 2000). The slope stability by vegetation is also governed by the hydro-mechanical properties of the root-soil matrix (Ghestem, Sidle, & Stokes 2011). Another example is the so-called vadoze zone (above the phreatic zone) where water is retained by adhesion and capillary action without being necessarily saturated. The properties of this zone are essential for agriculture and pollution transport. In the same way, the hydro-textural evolution of wetted granular materials is an important problem in industrial processes such as wet mixing and agglomeration of ores and powders (Ruiz, Rondet, Delalonde, & Desfours 2011).

An outstanding effect of liquid is the bulk cohesion induced by surface tension in a partially wetted granular material. The stability of a sand castle, for example, is ensured by small amounts of water distributed in the form of menisci that hold the grains together at their contact points (Richefeu, El Youssoufi, & Radjai 2006). The shear strength increases rapidly in this *pendular state* until all contacts between neighboring grains are wetted. Beyond this point, the cohesive strength of the material remains nearly independent of the amount of liquid. Further increase of liquid volume leads, however, to liquid clustering and increasing number of grains fully immersed in the liquid phase. Little is known about the distribution of liquid in this *funicular state* and the dependence of cohesion on the amount of liquid (Mitarai & Nori 2006).

Recent experiments show that the pore-filling process in transition to the funicular state is a rich and interesting physics problem involving an intricate texturing of liquid clusters (Scheel, Seemann, Brinkmann, Di Michiel, Sheppard, Breidenbach, & Herminghaus 2008). The intermediate states in the funicular state and transition to a fully saturated state have been characterized only through experimental retention curves and the authors are aware of no experimental studies of shear strength and liquid distribution in late funicular states at the scale of the disordered granular structure (Mitchell & Soga 2005).

In this paper, we are interested in the statistics of

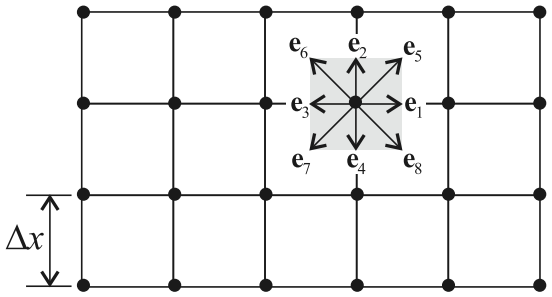

Figure 1: Lattice Boltzmann discretization of space and D2Q9 model.

liquid clusters in 2D granular packings as a function of an increasing amount of liquid distributed homogeneously inside the packing. We use a single-component multi-phase Lattice Boltzmann model together with a classical phase diagram in order to condense the liquid from a vapor phase injected numerically inside a periodic granular packing of disks. Unlike mechanical mixing, this method leads to a homogeneous distribution of liquid bridges between grains at thermodynamic equilibrium so that meaningful statistics can be obtained even with a low number of grains. By slowly increasing the amount of vapor, we obtain different clustering states: the pendular state at low liquid content, the funicular state in the intermediate range of liquid content and the bubble state at high liquid content. We investigate in detail the statistics of liquid clusters and the mean Laplace pressure as a function of the amount of liquid.

In the following, we first describe the modelling approach and simulated system. Then, we present a detailed analysis of the liquid clusters and their connection with the evolution of Laplace pressure as a function of the amount of liquid. We conclude with a short discussion and scopes of this work.

2 NUMERICAL METHOD AND SYSTEM DESCRIPTION

Partially saturated states in a granular material involve three phases: solid grains, liquid and gaz. Hence, a numerical or theoretical model requires three ingredients: 1) granular dynamics, 2) Navier-Stokes equations for the liquid, and 3) thermodynamics of gas-liquid phase transition (including surface tension). The fluid is simulated by means of the Lattice Boltzmann Method (LBM), which consists in discretizing the Boltzmann equation in the phase space and time using a finite difference scheme. In this work, we use the two-dimensional D2Q9 model with nine discrete velocities on a square grid of spacing Δx (Fig. 1).

In this model, discrete velocities are defined along 8 possible directions of motion from a node to its 8 surrounding neighbors. By denoting $c = \Delta x/\Delta t$ and $c_s = \frac{c}{\sqrt{3}}$ the propagation speed on the lattice, we set $\mathbf{e}_1 = (c, 0)$, $\mathbf{e}_2 = (0, c)$, $\mathbf{e}_3 = (-c, 0)$, $\mathbf{e}_4 = (0, -c)$ for the rectilinear directions, and $\mathbf{e}_5 = (c, c)$, $\mathbf{e}_6 = (-c, c)$, $\mathbf{e}_7 = (-c, -c)$, $\mathbf{e}_6 = (c, -c)$ for the diagonals directions and $\mathbf{e}_0 = (0, 0)$ in order to account for particles that stay in place at a node. The fluid flow is governed by the evolution equation:

$$f_a(\mathbf{x}_a, t + \Delta t) = f_a(\mathbf{x}, t) + \Omega_a + \Delta f_a \quad (1)$$

where the main variables f_a are the fluid particle distribution functions along different directions a, and $\mathbf{x}_a = \mathbf{x} + \mathbf{e}_a \Delta t$ denotes the nodes surrounding $\mathbf{x}$. The collision operator is based on the BGK approximation (Bhatnagar, Gross, & Krook 1954):

$$\Omega_a = \frac{\Delta t}{\tau}\left(f_a(\mathbf{x}, t) - \bar{f}_a(\mathbf{x}, t)\right) \quad (2)$$

with a single relaxation time τ. This collision term together with discretized Lattice-Boltzmann equation (1) leads to Navier-Stokes equations (Satoh 2011).

The fluid viscosity is computed through the relation $\nu = c_s \Delta t(\tau - \frac{1}{2})$ (Succi 2001). The equilibrium densities along lattice directions are given by the Maxwell distribution $\bar{f}_a(\mathbf{x}, t) = w_a \rho \left[1 + \frac{1}{c_s^2}\mathbf{e}_a \cdot \bar{\mathbf{u}} + \frac{1}{2c_s^4}\mathbf{e}_a \cdot \bar{\mathbf{u}}^2 - \frac{1}{2c_s^2}\bar{\mathbf{u}}^2\right]$, where the weight factor w_a is $4/9$ for $a = 0$, $1/9$ for $a = 1 \ldots 4$ and $1/36$ for $a = 5 \ldots 8$. For the computation, we use dimensionless Lattice Units (lu) with $\Delta t = 1$, $\Delta x = 1$ and $\tau = 1$. The body forces are applied through the relation $\Delta f_a = \bar{f}_a(\rho, \mathbf{u} + \Delta\mathbf{u}) - \bar{f}_a(\rho, \mathbf{u})$ with $\Delta\mathbf{u} = \mathbf{F}\Delta t/\rho$. The equilibrium velocity can be obtained from $\rho\bar{\mathbf{u}} = \sum_{a=0}^{8} f_a \mathbf{e}_a + \mathbf{F}\Delta t/2$, where ρ is the mass density at a node $\rho = \sum_{a=0}^{8} f_a$.

One major advantage of LBM is its ability to account for multiphase flows (He, Chen, & Zhang 1999, Sukop & Or 2004, Huang & Lu 2009). The interactions between liquid, gas and solid (grains) are derived using nonlocal potentials. These potentials are calculated on a regular mesh between the fluid particles and neighboring lattice nodes that control the surface tension and contact angle between fluid and solid (He & Doolen 2002). Long range inter-particle potentials to model multiphase flows were initially introduced by Shan and Chen (Shan 1993, Shan 1994) through a so called *effective mass* ψ reflecting the momentum change due to cohesion forces. In the early models of phase separation the function ψ was simply assumed to be an increasing function of density (Shan & Doolen 1995). Recently, different methods have been proposed through a thermodynamically founded equation of state (Swift 1996, He & Doolen 2002, Kupershtokh, Medvedev, & Karpov 2009). Most of these methods use the approximation $\psi(\mathbf{x}) = \sqrt{-2(p(\mathbf{x}) - c_s^2\rho(\mathbf{x}))/c_s^2}$ obtained through the Chapman-Enskog expansion, where p is the pressure at the node $\mathbf{x}$ (Yuan & Schaefer 2006).

In this paper, we consider the following expression of the body force (in which we account both for fluid internal cohesion and fluid-solid adhesion):

$$\mathbf{F}(\mathbf{x}) = \psi(\rho(\mathbf{x}))\sum_{a=0}^{8} w_a[\psi(\rho(\mathbf{x}))(1 - s(\mathbf{x}_a)) + \psi(\rho_{fs}(\mathbf{x}))s(\mathbf{x}_a)]\mathbf{e}_a \quad (3)$$

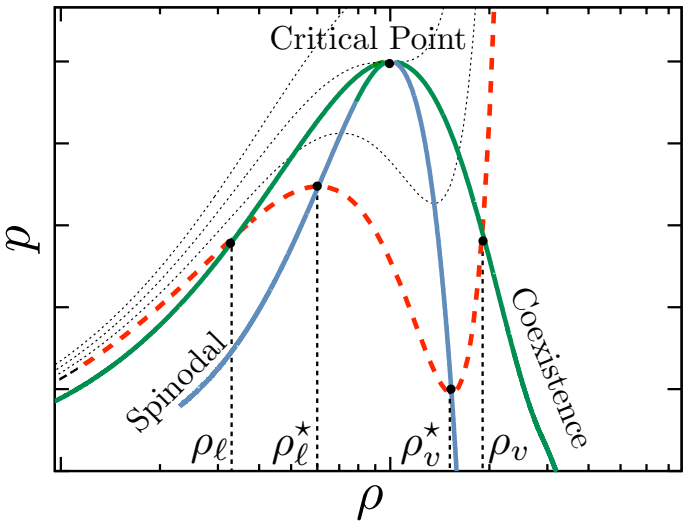

Figure 2: Isotherm (dotted line), coexistence and spinodal curves according to Carnahan-Starling's equation of state. The pressures and densities are normalized by those of the triple point.

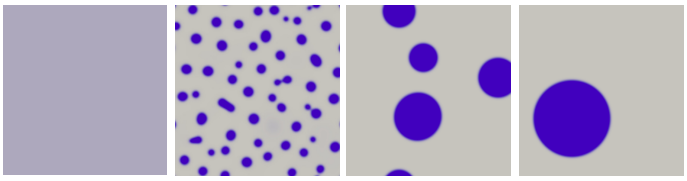

Figure 3: From left to right: condensation and coalescence of liquid drops at constant volume.

where s is an indicator function, equal to 1 if the node is solid and 0 otherwise, and $\rho_{fs}(\mathbf{x})$ is used to modify the contact angle at the fluid-solid interface by choosing a value between gas and liquid densities at the solid nodes (Huang, Li, Liu, & Lu 2008).

The thermodynamics of phase change is based on Carnahan-Starling's equation of state (Kupershtokh, Medvedev, & Karpov 2009), which is an improvement of the classical van der Waals equation; see Fig. 2. It can be written using the variables p, ρ and T, which are normalized here by their values at the critical point:

$$p = c\rho T \frac{1 + b\rho + (b\rho)^2 - (b\rho)^3}{(1 - b\rho)} - a\rho^2 \qquad (4)$$

where $a = 3.8525$, $b = 0.1304$ and $c = 2.7859$ are fixe parameters obtained by solving the system of 3 equations: $\left\{p = 1\ ;\ \frac{\partial p}{\partial \rho}\Big|_{\tilde{T}} = 0\ ;\ \frac{\partial^2 p}{\partial^2 \rho}\Big|_{T} = 0\right\}$ at critical point $(\rho = 1; T = 1)$ (Kupershtokh, Medvedev, & Karpov 2009). It is worth noting that in this model all free parameters are fixed by setting the values of the critical point.

For the LBM computation we set the critical values to $Pc = 0.00442\,\text{lu}$, $Tc = 0.0943\,\text{lu}$ and $\rho_c = 0.13044\,\text{lu}$ (Yuan & Schaefer 2006). Capillary condensation is triggered by setting the temperature to $T = 0.7T_c$ (see Fig. 2), and a uniform fluid density equal or greater than the minimum spinodal density $\rho_v^\star$. Practically, for simulations we use a fully periodic domain to which we add small fluctuations in the density field to initiate the coalescence process

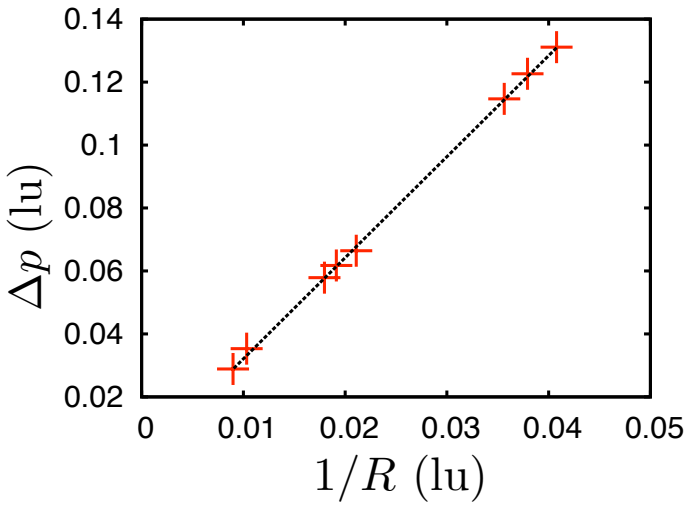

Figure 4: Evolution of pressure drop across the liquid-gas interface as a function of radii of 8 simulated drops and bubbles.

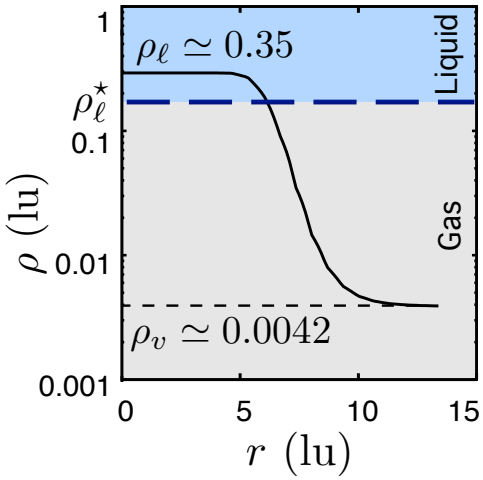

Figure 5: Evolution of fluid density across the liquid-gas interface as a function of distance r in units of lattice step Δx.

(Fig. 3). By varying the amount of liquid, it is possible to get drops or bubbles of different sizes and to determine liquid-vapor surface tension $\gamma_{\ell v} \simeq 0.014$ lu from Laplace equation, as shown in Fig. 4. In the simulations reported below, the wetting contact angle is set to zero. Physically, this is equivalent to setting $\gamma_{sv} = \gamma_{\ell v}$, where γ_{sv} is the solid-vapor surface tension. The fluid density ρ at the interface between bulk liquid and bulk gas varies fast but smoothly over a few lattice steps. Figure **??** shows the evolution of ρ across a liquid-vapor interface.

The granular samples are prepared by isotropic compaction of 1000 disks with a friction coefficient $\mu = 0.1$ simulated by the molecular dynamics method inside a biperiodic cell (Radjai & Dubois 2011). The grains have a uniform size distribution by volume fractions with a ratio 3 between the largest and smallest grains. The resulting static configuration has a packing fraction 0.82 and a coordination number 5.6. The space is meshed by a rectilinear grid of 2 250 000 nodes, corresponding to at least 30 nodes within a small grain diameter. Furthermore, since in 2D the pores are closed, we added a thin permeable layer around each grain to allow for fluid transfer in the pore space. This is important for fast relaxation of

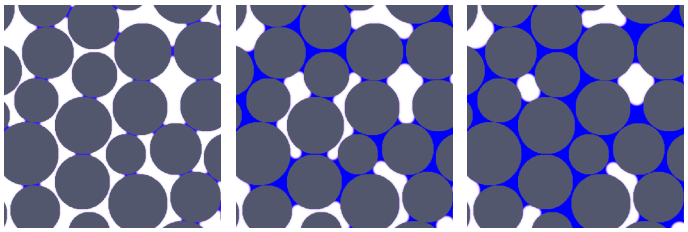

Figure 6: Snapshots of liquid clusters with increasing amount of liquid. From left to right, $S = 0.1$, $S = 0.3$ and $S = 0.7$.

thermodynamic variables to equilibrium although the vapor is introduced randomly in all pores.

The evolution of liquid clusters and internal stresses or pressures are monitored as a function of the saturation degree S, defined as the volume V_{liquid} of condensed liquid normalized by the total pore volume V_{pores}, using a floodfill algorithm. This classical digital image processing algorithm allows one to determine the area connected to each seed node. By using the contact points between grains as the initial seeds, we determine all independent clusters in the system for all values of S. In all simulations reported in this paper, the grains are fixed, implying that the capillary forces resulting from liquid-gas surface tension acting at the triple points on the grains and Laplace pressure acting at the liquid-grain interface are fully balanced by the contact forces exerted by the neighboring grains of each grain.

The natural physical units of the system are the grain size d, liquid density ρ_ℓ and liquid-vapor surface tension $\gamma_{\ell v}$. Hence, in the following we normalize the lengths by d, the forces by $\gamma_{\ell v}$ and the stresses by $\gamma_{\ell v}/d$. Note that in 2D the surface tension is understood as "line tension" with the dimension of a force.

Animation videos of the simulations can be found at the following address: `www.cgp-gateway.org/Video/Wet_Packing`.

3 LIQUID CLUSTERING

Figure 6 displays three snapshots of liquid clusters with increasing degree of saturation S. Snapshot (a) corresponds to the pendular state where the liquid is distributed in the form of binary bridges between grains. Snapshot (b) represents a typical example of the early stages of the funicular state where liquid clusters are connected to two or more grains whereas snapshot (c) represents the latest stages of the funicular regime where a large number of grains are immersed in the liquid phase. Snapshot (d) corresponds to a high amount of liquid where the liquid clusters percolate throughout the packing and the mixture can be more appropriately described in terms of the distribution of grains and bubbles in a liquid.

The clustering state may be characterized by the proportion C_m of liquid clusters connected to m grains. In the same way, the grain environments can be described from the proportion P_n of grains connected to n independent liquid clusters. We will refer

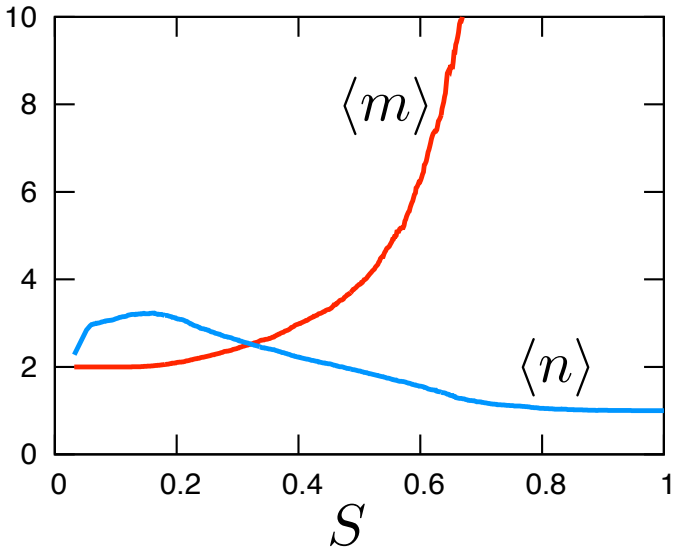

Figure 7: Evolution of the average clustering order $\langle m \rangle$ and wet coordination number $\langle n \rangle$ as a function of the amount of liquid.

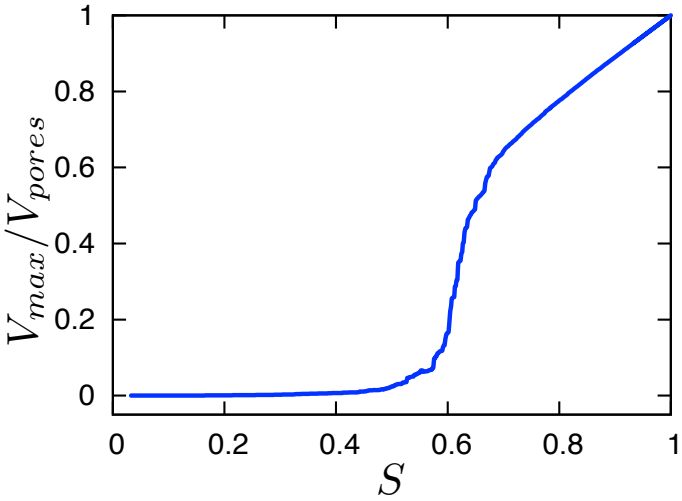

Figure 8: Evolution of the normalized volume V_{max}/V_{pores} of the largest liquid cluster as a function of the amount of liquid S.

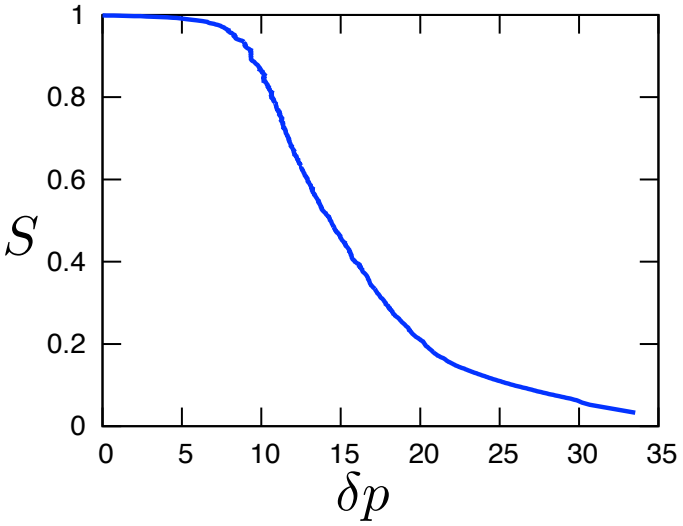

Figure 9: The amount of liquid S versus Laplace pressure difference $\delta p = p_v - p_\ell$, where p_v is the mean vapor pressure and p_ℓ is the mean liquid (negative) pressure. The pressures are normalized by $\gamma_{\ell v}/d$.

to m as the "order" of a cluster. The average state of liquid connectivity is given by the average clustering order $\langle m \rangle = \sum_{m=2}^{m_{max}} mC_m$ and the "wet" coordination number is $\langle n \rangle = \sum_{n=1}^{n_{max}} nP_n$. Figure 7 shows the evolution of $\langle m \rangle$ and $\langle n \rangle$ as a function of the amount of liquid S. In the pendular state, we have $\langle m \rangle = 2$. As the amount of liquid increases, liquid clusters of increasing order are formed by the coalescence of clusters of lower order. As a result, $\langle m \rangle$ begins to increase slowly from 2 at $S \geq 0.15$ and diverges around $S = 0.6$. As we shall see below, this point corresponds to the percolation transition of the liquid phase.

The wet coordination number $\langle n \rangle$ increases in the pendular state from zero to a maximum ($\simeq 3.5$ at $S \simeq 0.15$) corresponding to the largest number of binary liquid bridges. Then, it declines down to $\langle n \rangle \simeq 1$ at $S \simeq 0.8$, which corresponds to a state where most grains are either immersed in liquid or in contact with the percolating liquid cluster and a binary bridge; see Fig. 6(d).

A percolation transition occurs in the liquid phase at $S \simeq 0.6$ as seen in Fig. 8 where the volume of the largest cluster V_{max} normalized by the total pore volume V_{pores} is plotted as a function of S. Note that the process of the coalescence of primary liquid clusters begins well before with an increasing number of immersed grains. After transition, the liquid phase forms a single cluster and we have $V_{max}/V_{pores} \simeq S$. The percolation transition reveals the highly nonlinear character of the pore-wetting process although the distribution is homogeneous in the bulk. This feature is a reflection of granular disorder. The fact that the transition occurs far below full saturation ($S = 1$) means that the liquid can exist as a continuous phase without filling the pores.

The macroscopic states of water in soils are generally classified by considering the relationship between water content S, and the Laplace pressure difference (or suction) $\delta p = p_v - p_\ell$, where p_v is the mean vapor pressure and p_ℓ is the mean liquid (negative) pressure. This *retention curve* is used to characterize different types of soil (depending on the grain size and shape distributions), but it has a generic form that is quite well reproduced by our simulations, as shown in Fig. 9. The two ranges $S < 0.15$ and $S > 0.9$ can be distinguished from the intermediate regime where S increases rapidly as δp declines with practically no signature of the percolation transition evidenced for the largest liquid cluster in Fig. 8.

The largest values of δp occur at the very early stages of the pendular state with small values of the radius of curvature of the capillary bridges. In our simulations, as a result of the permeable layer introduced at the contact points allowing for fluid transfer between pores in 2D, the largest value (in absolute value) of δp reflects the minimal gap between grains. Up to $S \simeq 0.15$, the Laplace pressure declines almost linearly as S increases as a result of the increase of the radius curvature of the capillary bridges.

4 DISCUSSION

In this paper, LBM simulations of homogeneous capillary condensation were used create homogeneous distributions of a liquid in the form of capillary bridges clusters. We introduced the numerical method and analyzed the clustering of liquid and the evolution of Laplace pressure as a function of the amount of liquid in a 2D granular packing. The coalescence of binary bridges begins for a degree of saturation $S \simeq 0.15$ where the mean order $\langle m \rangle$ of liquid clusters begins to increase whereas the volume of the largest cluster remains nearly constant up to $S \simeq 0.6$. This shows that the funicular state in this range may simply be seen as a juxtaposition of hardly touching binary bridges, in agreement with the experiments of Scheel et al. (Scheel, Seemann, Brinkmann, Di Michiel, Sheppard, Breidenbach, & Herminghaus 2008). The largest cluster begins to grow after this primary phase of coalescence and the liquid clusters percolate throughout the system. In this late funicular state, an increasing number of grains are immersed in the liquid and the vapor phase is in the form of bubbles connected to two or more grains.

The Laplace pressure declines during saturation as a function of S with a shape very similar to measured retention curves in soil mechanics. The evolution of the connectivity of liquid clusters evidenced by simulations in this work for all degrees of saturation (from binary bridges to full saturation of pores) indicates that four states should be distinguished in the description of unsaturated soils: 1) pendular state, corresponding to binary liquid bridges, 2) primary funicular state, where the capillary bridges join one another without filling the volume, 3) secondary funicular state, where the liquid volume percolates and many particles are fully immersed, 4) bubble state, characterized by bubbles connected to two or more

grains. This work will be pursued in order to evaluate the evolution of the internal cohesion of the fluid-grain mixture, which determines its cohesive strength. In particular, a pending issue is whether the cohesive strength increases within the funicular range as the amount of liquid increases and at for what level of saturation its peak value occurs.

REFERENCES

Bhatnagar, P. L., E. P. Gross, & M. Krook (1954). A model for collision processes in gases. I. small amplitude processes in charged and neutral one-component systems. *Physical Review 94*(3), 511–525.

Ghestem, M., R. C. Sidle, & A. Stokes (2011, Nov). The influence of plant root systems on subsurface flow: Implications for slope stability. *Bioscience 61*(11), 869–879.

He, X., S. Chen, & R. Zhang (1999, JUL 1). A lattice boltzmann scheme for incompressible multiphase flow and its application in simulation of rayleigh-taylor instability. *Journal of Computational Physics 152*(2), 642–663.

He, X. & G. D. Doolen (2002). Thermodynamic foundations of kinetic theory and lattice boltzmann models for multiphase flows. *J. Stat. Phys. 107*, 309–328.

Huang, H., Z. Li, S. Liu, & X. Lu (2008). Shan-and-chen-type multiphase lattice boltzmann study of viscous coupling effects for two-phase flow in porous media. *International Journal for Numerical Methods in Fluids 61*(3), 341–54.

Huang, H. & X. Lu (2009). Relative permeabilities and coupling effects in steady-state gas-liquid flow in porous media: A lattice boltzmann study. *Physics of Fluids 21*(9), 092104.

Iverson, R. M., M. E. Reid, N. R. Iverson, R. G. LaHusen, M. Logan, J. E. Mann, & D. L. Brien (2000, Oct). Acute sensitivity of landslide rates to initial soil porosity. *Science 290*(5491), 513–516.

Kupershtokh, A., D. Medvedev, & D. Karpov (2009). On equations of state in a lattice boltzmann method. *Comput. Math. Appl. 58*(5), 965 – 974.

Mitarai, N. & F. Nori (2006, Jan-Apr). Wet granular materials. *Adv. in Physics 55*(1-2), 1–45.

Mitchell, J. & K. Soga (2005). *Fundamentals of Soil Behavior*. NY: Wiley, New-York.

Radjai, F. & F. Dubois (Eds.) (2011). *Discrete-element Modeling of Granular Materials*. Wiley.

Richefeu, V., M. S. El Youssoufi, & F. Radjai (2006, May). Shear strength properties of wet granular materials. *Phys. Rev. E 73*(5), 051304.

Ruiz, T., E. Rondet, M. Delalonde, & J. P. Desfours (2011, Mar). Hydro-textural and consistency surface states of humid granular media. *Powder Technol. 208*(2), 409–416.

Satoh, A. (2011). *Introduction to practice of molecular simulation*. Elsevier.

Scheel, M., R. Seemann, M. Brinkmann, M. Di Michiel, A. Sheppard, B. Breidenbach, & S. Herminghaus (2008, Mar). Morphological clues to wet granular pile stability. *Nat. Mater. 7*(3), 189–193.

Shan, X. (1993). Lattice boltzmann model for simulating flows with multiple phases and components. *Physical Review E 47*(3), 1815–1819.

Shan, X. (1994). Simulation of nonideal gases and liquid-gas phase transitions by the lattice boltzmann equation. *Physical Review E 49*(4), 2941–2948.

Shan, X. & G. Doolen (1995). Multicomponent lattice-boltzmann model with interparticle interaction. *Journal of Statistical Physics 81*, 379–393.

Succi, S. (2001). *The Lattice Boltzmann Equation For Fluid Dynamics and Beyond*. Oxford University Press.

Sukop, M. & D. Or (2004). Lattice boltzmann method for modeling liquid-vapor interface configurations in porous media. *Water Resources Research 40*, W01509.

Swift, M. (1996). Lattice boltzmann simulations of liquid-gas and binary fluid systems. *Physical Review E 54*(5), 5041–5052.

Yuan, P. & L. Schaefer (2006). Equations of state in a lattice boltzmann model. *Physics of Fluids 18*, 042101.